Superconducting properties of $La_3Ni_2B_2N_{3-\delta}$

H. Michor
Institut für Experimentalphysik, Technische Universität Wien, Wiedner Hauptstrasse 8-10, A-1040 Wien, Austria

R. Krendelsberger
Institut für Physikalische Chemie, Universität Wien, Währingerstrasse 42, A-1090 Wien, Austria

G. Hilscher, E. Bauer, C. Dusek, R. Hauser, L. Naber, and D. Werner
Institut für Experimentalphysik, Technische Universität Wien, Wiedner Hauptstrasse 8-10, A-1040 Wien, Austria

P. Rogl
Institut für Physikalische Chemie, Universität Wien, Währingerstrasse 42, A-1090 Wien, Austria

H. W. Zandbergen
National Centre for High Resolution Electron Microscopy (HREM), Laboratory of Materials Science, Delft University of Technology, Rotterdamseweg 137, 2628 AL Delft, The Netherlands

(Received 4 June 1996)

Nearly-single-phase $La_3Ni_2B_2N_{3-\delta}$ prepared by arc melting and subsequent annealing at 1100 °C is characterized by x-ray powder techniques, electron microprobe analysis, and high-resolution electron microscopy. A standardized set is provided for the crystallographic parameters, and structural chemistry is described from the point of view of nonmetal-nonmetal interactions as well as of the metal coordination around the nonmetal atoms. The superconducting properties of $La_3Ni_2B_2N_{3-\delta}$ are studied by means of resistivity, magnetization, and heat capacity measurements. The obtained critical fields $\mu_0 H_c(0)=0.16$ T, $\mu_0 H_{c1}(0)=13(2)$ mT, and $\mu_0 H_{c2}(0)=7.5(5)$ T classify $La_3Ni_2B_2N_{3-\delta}$ as a hard type-II superconductor with a Ginzburg-Landau parameter $\kappa=33(2)$, a coherence length $\xi_0=7.0(5)$ nm, and a penetration depth $\lambda(0)$ of about 210 nm. The pressure dependence of T_c with $dT_c/dp=-130$ mK/kbar is found to be one order of magnitude larger than for RNi_2B_2C (R=Y, Lu). Since the deviations of the thermodynamic ratios as $\Delta C/\gamma T_c$, $\gamma T_c^2/H_c^2(0)$, $H_c(0)/H_c'(T_c)T_c$, and $\Delta(0)/k_B T_c$ from their BCS values are rather small, $La_3Ni_2B_2N_{3-\delta}$ is characterized as a phonon-mediated weak- to medium-coupling BCS superconductor. [S0163-1829(96)01638-4]

I. INTRODUCTION

The discovery of superconductivity in $LuNi_2B_2C$ and other quaternary lanthanide transition-metal borocarbides with critical temperatures T_c up to 23 K (Refs. 1–3) stimulated the search for further intermetallic superconductors with layered crystal structures. Recently, Cava and co-workers[4,5] reported new lanthanum nickel boronitrides $(LaN)_nNi_2B_2$ with $n=2, 3$ which are isostructural with the homologous borocarbide series $(YC)_nNi_2B_2$ ($n=1, \ldots,4$).[5–7] The structure of these compounds is body-centered tetragonal and consists of Ni_2B_2 layers built from NiB_4 tetrahedra separated by n LaN or YC rocksalt-type layers. For the series $(YC)_nNi_2B_2$ ($n=1, \ldots,4$) superconductivity could only be found for single-layer YNi_2B_2C ($T_c \simeq 15$ K) whereas all others ($n>1$) are nonsuperconducting down to 4.2 K.[7] Thus, it was speculated that the close contact of Ni_2B_2 layers in YNi_2B_2C is a prerequisite for the appearance of superconductivity. In the new quaternary boronitrides, however, superconductivity is observed for $La_3Ni_2B_2N_3$ ($T_c \simeq 12$ K) where three LaN rocksalt-type layers separate the Ni_2B_2 layers. The two-layer compound LaNiBN is reported to be nonsuperconducting down to 4.2 K.[4] Recently, superconductivity up to 8.9 K was also reported for the pseudoquaternary two-layer borocarbides $Y(Ni_{1-x}Cu_x)BC$ and $Lu(Ni_{1-x}Cu_x)BC$ by Gangopadhyay and Schilling.[8]

The interesting question of whether the separation of the Ni_2B_2 layers by three LaN rocksalt layers gives rise to a more two-dimensional character (as evidenced for many high-T_c cuprates) was investigated via band structure calculations by Singh and Pickett[9] and Mattheiss.[10] They suggest that the electronic properties are rather three dimensional.

The aim of the present paper is to characterize the thermodynamic properties of the superconducting state of $La_3Ni_2B_2N_{3-\delta}$ and to compare the obtained results with those of the single-layer borocarbide superconductors RNi_2B_2C (R=Y, Lu).

II. EXPERIMENT

Polycrystalline samples were synthesized by arc melting on a water-cooled copper hearth using a tungsten electrode. The starting materials were lanthanum ingots (Auer-Remy, D, 99.9%), Ni powder or ingots (Alfa-Ventron, D, 99.9%), and hexagonal boron nitride powder (Johnson Matthey & Co., GB, 99.8%), which was compacted to a small pellet prior to use. In a first step, Ni and La were melted together in an Ar atmosphere to produce a master alloy, which then was reacted with the boron nitride pellet by dissolving it into the

(La,Ni) melt heated by the arc. Reactions of La with pellets made of Ni and BN powder resulted in rather poor specimens. To ensure homogeneity the alloy buttons were broken and remelted under Ar for several times. After changing the gas in the arc-melting furnace to nitrogen (99.999%) the broken reguli were remelted again for several times. Alternatively the first melting step, particularly of the La ingot, has been carried out under nitrogen, and although this method proved to be more difficult to prevent exothermic spitting of the melt, a higher success rate in obtaining single-phase products was achieved.

Rather large samples (≈3.5 g) used for the specific heat measurements were prepared in a final melting run under nitrogen from individually homogenized smaller pellets, each of about 1.5 g. For annealing, the samples were wrapped in protective Mo foil, sealed in evacuated silica capsules, and heated for 150 h at 1100 °C.

It should be mentioned that heat treatments, i.e., at 900 °C under 10^5 Pa nitrogen, resulted in a pronounced formation of LaN. Due to the high sensitivity of LaN to moisture, LaN-containing samples decomposed quickly in air, while phase pure bulk $La_3Ni_2B_2N_{3-\delta}$ revealed a remarkable stability and hardly changed even when stored for several weeks under normal laboratory conditions. A small quantity of each sample was powdered under cyclohexane, sealed in thin quartz capillaries and exposed to Cr $K\alpha$ radiation ($\lambda K\alpha_1 = 0.228\ 970$ nm) in a Debye-Scherrer camera ($R = 57.296$ mm). Precise lattice parameters were determined by means of a least squares refinement of Guinier-Huber photographs with Cu $K\alpha_1$ radiation ($\lambda = 0.154\ 056\ 2$ nm) using an internal Ge standard $a_{Ge} = 0.565\ 790\ 6$ nm.

A quantitative electron microprobe (EMP) analysis was performed on a CAMEBAX SX 50 wavelength dispersive spectrograph comparing the $K\alpha$ emissions of the elements B, N, Ni, and the $L\alpha$ of La with those from standards of elemental Ni, VN, and $LaB_{5.85}$. A deconvolution of Ni and La had to be applied in addition to the general correction procedure.[11] The experimental parameters employed were acceleration voltage of 15 kV, sample current of 15 nA, and spectrometer crystals such as PET for La $L\alpha$, LiF for Ni $K\alpha$, PC3 for B $K\alpha$, and PC1 for the N $K\alpha$.

Electron transparent areas of the specimens were obtained by crushing under dry isopropanol, mounting the crushed particles on a carbon-coated holey film, and then transferring them into the electron microscope as quickly as possible. High-resolution electron microscopy (HREM) was performed with a Philips CM30ST electron microscope with a field emission gun and Link energy-dispersive x-ray (EDX) equipment operated at 300 kV.

Resistivity measurements in external magnetic fields up to 14 T were carried out in a conventional ^{3}He cryostat

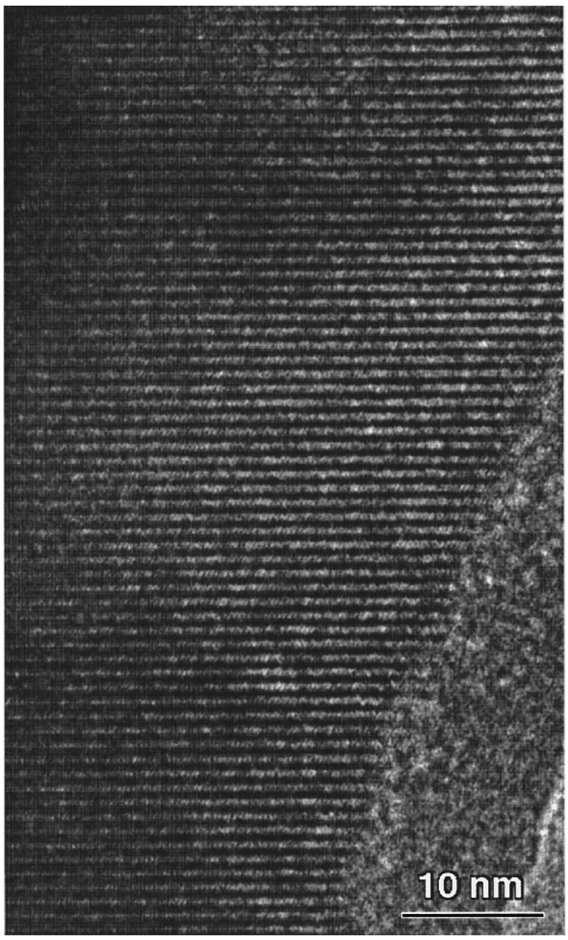

FIG. 1. Low-resolution micrograph of $La_3Ni_2B_2N_{3-\delta}$ showing the absence of (planar) defects.

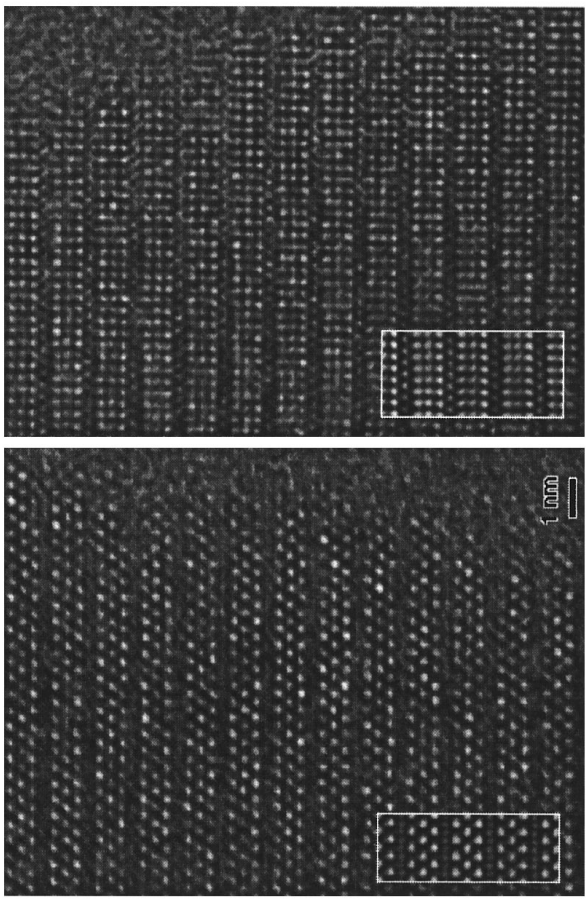

FIG. 2. HREM images of $La_3Ni_2B_2N_{3-\delta}$ along [100] (lower) and [110] (upper). Averaged images are shown as insets. The bright dots represent the La and Ni positions. The two images are aligned in vertical direction such that Ni planes occur at the same height.

(300 mK to 100 K) using a calibrated CERNOX temperature sensor. Additionally, zero-field measurements were performed up to room temperature. High-pressure resistivity measurements up to 12 kbar were performed in a liquid pressure cell with a 4:1 methanol-ethanol mixture as pressure-transmitting medium. All resistivity measurements were performed on bare-shaped samples employing a four-probe dc method.

ac- and dc-susceptibility measurements were performed in a calibrated ac susceptometer (80 Hz and field amplitudes up to 1 mT) and in a 6 T superconducting quantum interference device (SQUID) magnetometer, respectively.

Specific heat measurements up to 11 T were carried out on 2 – 3 g samples in the temperature range 1.5–100 K and in zero magnetic field from 80 to 300 K. Both experiments employ a quasiadiabatic step heating technique.

III. RESULTS

A. Compound formation and structural chemistry

The quantitative analysis of the polycrystalline $La_3Ni_2B_2N_{3-\delta}$ sample by EMP essentially revealed rather stoichiometric $La_3Ni_2B_2N_3$ as the bulk phase intergrown with a few small areas of LaNiBN and with a few small particles of nitrogen-free ternary lanthanum nickel borides. From a line scan of more than 500 individually measured points in intervals of 2 μm we observe a variation of the N content between 25 and 30 at. % whereas the corresponding variation of the B, Ni, and La concentrations was less than 2 at. % in each case. In a further investigation of the microstructure of $La_3Ni_2B_2N_{3-\delta}$ by transmission electron microscopy about 200 small crystals (0.5–5 μm) were analyzed by EDX. All crystals had a La/Ni ratio which is consistent with the composition $La_3Ni_2B_2N_3$ except for one which could be identified as LaNiBN. Crystals of the phase $La_3Ni_2B_2N_{3-\delta}$ were studied by HREM to check whether any planar defects do occur. All crystals investigated did not show any planar defects. About 30 crystals with an average size of 5 μm were investigated such that on a length scale of 0.15 μm along the *c* axis no stacking fault was observed, suggesting that the density of these defects is less than 10 ppm and thus not relevant for the physical properties. The difference of this specimen with $La_3Ni_2B_2N_{3-\delta}$ prepared with rather short annealing times is remarkable. Whereas in the latter specimens many planar defects do occur,[5] such defects are absent in the present specimen, as in other specimens annealed for a relatively long time.

Figure 1 shows a transmission electron microscopy (TEM) image of $La_3Ni_2B_2N_{3-\delta}$ in [100] which is typical for the material; no planar defect is present in this image. Figure 2 shows HREM images along [100] and [110]. In the [100] image the typical three rows of bright dots due to La atoms in the triple LaN layers. The Ni atoms are imaged less dominant (due to a smaller scattering potential and a short distance between the Ni columns) but in the averaged image they appear as bright dots too. In the [110] image the Ni and La atoms are imaged approximately equally bright due to a ratio of two Ni atoms per one La atom.

X-ray photographs of the alloy specimens prepared according to the description given in Sec. II revealed an intensity pattern which was successfully and completely indexed on the basis of the crystal structure of $La_3Ni_2B_2N_3$ (see Ref. 12) in combination with small amounts of secondary phases (mainly unreacted BN; traces of LaNiBN found in the

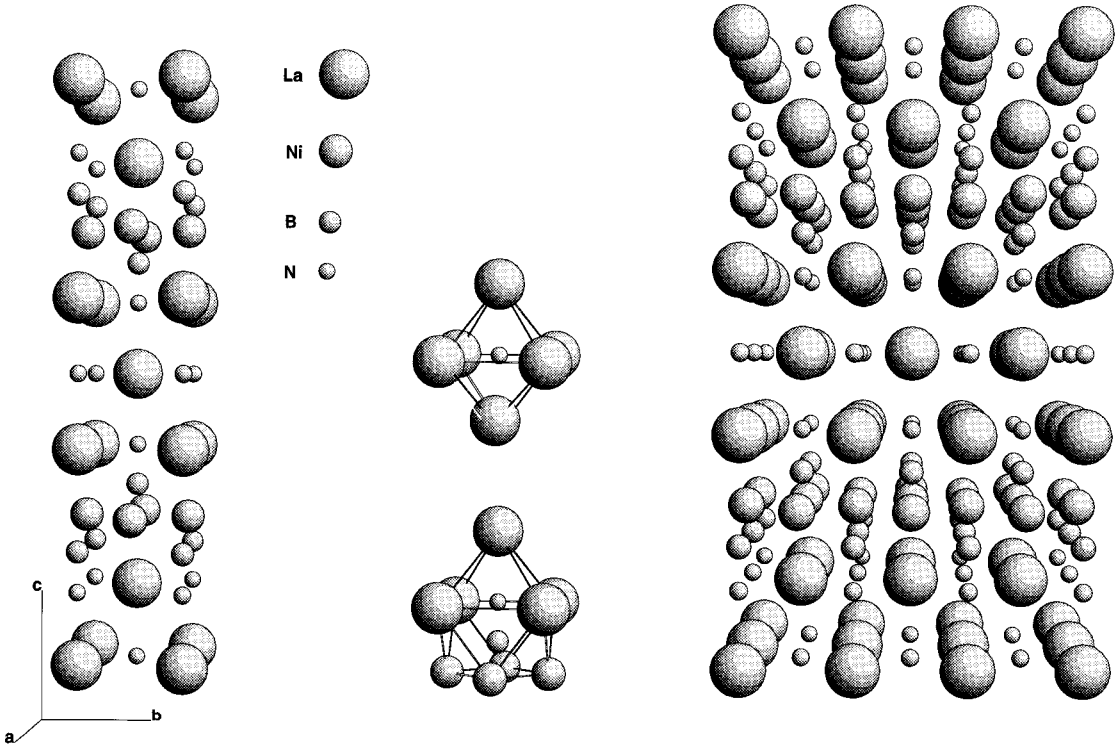

FIG. 3. The crystal structure of $La_3Ni_2B_2N_3$ in a three-dimensional perspective view.

TABLE I. Crystallographic data of $La_3Ni_2B_2N_{3-\delta}$ [standardized setting, calculated by the program STRUCTURE TIDY (Ref. 15) using the crystallographic data given in Ref. 12].

Lattice parameters	$a=0.37207(6)$ nm, $c=2.0514(6)$ nm, $V=0.2840(1)$ nm^3, $c/a=5.514$					
Space group	$I4/mmm$, No. 139, origin at center, $Z=2$					
Structure type	$La_3Ni_2B_2N_3$					
Atom parameters, standardized setting	Atom	Site	x	y	z	Occupation
	N1	4e	0.0000	0.0000	0.1246	1.00
	B	4e	0.0000	0.0000	0.1946	1.00
	La1	4e	0.0000	0.0000	0.3705	1.00
	Ni	4d	0.0000	0.5000	0.2500	1.00
	N2	2b	0.0000	0.0000	0.5000	0.91
	La2	2a	0.0000	0.0000	0.0000	1.00

Interatomic distances (nm)	Central atom: N1		Central atom: B		Central atom: La1	
	Ligand atoms	Distances (nm)	Ligand atoms	Distances (nm)	Ligand atoms	Distances (nm)
	1 B	0.1436	1 N1	0.1436	4 N1	0.2632
	1 La2	0.2556	4 Ni	0.2179	1 N2	0.2656
	4 La1	0.2636	4 La1	0.2949	4 B	0.2949
					4 Ni	0.3093
					1 B	0.3608
					4 La1	0.3719
					4 La2	0.3738
	Central atom: Ni		Central atom: N2		Central atom: La2	
	Ligand atoms	Distances (nm)	Ligand atoms	Distances (nm)	Ligand atoms	Distances (nm)
	4B	0.2179	4 La2	0.2630	2 N1	0.2556
	4 Ni	0.2630	2 La1	0.2656	4 N2	0.2630
	4 La1	0.3093			4 La2	0.3719
					8 La1	0.3738
Bonding angles	N-B-Ni	Ni-B-Ni	Ni-B-Ni	B-Ni-B	B-Ni-B	N-B-La
	121.39°	74.25°	117.21°	117.21°	105.75°	63.08°

EMP analysis could not be resolved in the x-ray pattern). Using the atom positions as derived from a neutron powder diffraction study,[12] agreement between observed and calculated x-ray powder intensities is excellent.

The crystal structure of $La_3Ni_2B_2N_3$ as a member of the general family $(LaN)_m(NiB)_n$ is usually described as a combination of rocksalt LaN units with NiB-fluorite blocks. These structure descriptions usually focused on the coordination of the metal atoms. Proper classification of ternary metal borides, carbides, or nitrides, however, is usually based on the metal coordination around the nonmetal atoms (see Fig. 3). The classification of ternary metal borides including borocarbides and boronitrides was successful on the basis of the type of the boron-boron aggregation as a function of the metal to boron ratio.[13,14] In such a way the manifold of about 900 ternary representatives of borides crystallizing with about 130 various structure types is reduced to a mere of only three different structural units: (a) the Archimedian antiprism M_8B, (b) the trigonal prism M_6B eventually enlarged to a tetrakaidekahedral coordination $M_{6+3}B$ with three additional M atoms facing the rectangular prism faces, and (c) in rather rare occasions, i.e., for typical metal host structures, the octahedron M_6B. As typical for binary and ternary borides, the Archimedian antiprism is usually observed for the structure types M_2B to M_5B_3 and M_3B_2. This pattern not only holds for the $ThCr_2Si_2$-type borides but also for the series $(MN)_m(M'B)_n$, where the Archimedian antiprism again is the characteristic metal coordination $M_4M'_4B$ around the B atom for the LuNiBC, and YNi_2B_2C as well as for the $La_3Ni_2B_2N_3$ types. As usual tight Ni-B bonds are formed, while La-B bonds (0.295 nm) are slightly exceeding the sum of the atom radii ($R_B+R_{La}=0.274$ nm) when we take $a/2$ as the structure inherent La radius and 0.088 nm for the radius of the boron atom. In most of the hitherto known metal borocarbides and boronitrides, carbon and nitrogen atoms (if not isolated) are covalently bonded to the boron sublattice, forming either single, double, or even higher bond orders. As a consequence, carbon and nitrogen atoms when isolated are at the centers of triangular prisms or metal octahedra, when at-

tached to the boron sublattice, are found in a sixfold coordination where one boron atom assumes the remaining vertex of an octahedron which is thus rendered a tetragonal double pyramid $[M_5\mathrm{B}]\mathrm{N}$ or $[M_5\mathrm{B}]\mathrm{C}$. In these cases, the B, N nonmetal also appears to approach the center of the tetragonal metal pyramide M_5 out of the center of its basal square M_4. The B-N distance of 0.144 nm being rather short compared to a single-bond distance of $R_\mathrm{B}+R_\mathrm{N}=0.088+0.077=0.165$ nm ensures via a higher bond order a rather tight binding between the LaN units with N in $\mathrm{La}_6\mathrm{N}$ octahedra and the Archimedian antiprismatic $\mathrm{La}_4\mathrm{Ni}_4\mathrm{B}$ blocks. As typical for borides with $1<M/\mathrm{B}<2$, there is no direct B-B connectivity. A summary of the crystallographic data of $\mathrm{La}_3\mathrm{Ni}_2\mathrm{B}_2\mathrm{N}_{3-\delta}$ is given in Table I.

B. Magnetic and resistivity measurements

The temperature dependence of the magnetization upon zero-field and field cooling of a bulk $\mathrm{La}_3\mathrm{Ni}_2\mathrm{B}_2\mathrm{N}_{3-\delta}$ specimen with approximate dimensions of $0.5\times1\times2.5\ \mathrm{mm}^3$ is shown in Fig. 4(a) for applied fields of 3 mT and 30 G. In the low-field limit (3 mT) the shielding signal is in good agreement with the value expected for perfect diamagnetism (using the theoretical density of $6.99\ \mathrm{g/cm}^3$ and the correction for demagnetization of the macroscopic sample geometry, $D\sim0.15$). The irreversibility upon field and zero-field cooling is typical for hard type-II superconductivity. The Meissner ratio attains 16% at 0.1 T similar to the borocarbides.

Isothermal magnetization measurements were performed subsequent to zero-field cooling of the sample. The lower critical field μ_0H_{c1} at various temperatures was first determined as the field where M deviates from the linear M-H relationship. The obtained result was additionally checked by measuring minor isothermal hysteresis loops to progressively higher magnetic fields. The field at which the loop begins to open indicates flux penetration and, hence, the upper limit of the Meissner state.

The magnetization loop determined at 2 K is shown in Fig. 4(b). The initial part of the magnetization $M(H)$ at various temperatures is displayed in Fig. 4(c). Analyzing the deviations of $M(H)$ from linearity, we obtain an estimate for the lower critical field at zero temperature, $\mu_0H_{c1}(0)=13(2)$ mT. The upper critical field μ_0H_{c2} was studied by means of resistivity and specific heat measurements because H_{c2} exceeds the field regime covered by magnetic measurements.

The electrical resistivity ρ of $\mathrm{La}_3\mathrm{Ni}_2\mathrm{B}_2\mathrm{N}_{3-\delta}$ (measured in zero magnetic field) is shown in Fig. 5. The resistive transition temperature $T_c^\rho=12.25(5)$ K is determined by the mean of the temperatures corresponding to 10% and 90% of the resistive jump. The difference between these temperatures yields a transition width of 0.6 K. The normal state resistivity $\rho(T)$ can be accounted for by the Bloch-Grüneisen relation

$$\rho(T)=\rho_0+\frac{4B}{\Theta_D}\left(\frac{T}{\Theta_D}\right)^5\int_0^{\Theta_D/T}\frac{z^5dz}{(e^z-1)(1-e^{-z})}. \quad (1)$$

A least squares fit according to this model (shown as the solid line in Fig. 5) yields an electron-phonon coupling constant $B=8.52\ \mathrm{m\Omega\ cm\ K}$, a Debye temperature $\Theta_D^\rho=330$ K, and a residual resistivity ρ_0 of 9.5 $\mu\Omega$ cm. The latter value is slightly too high because the low-temperature part of $\rho(T)$ is not properly described.

The suppression of superconductivity with rising external magnetic fields monitored by resistivity measurements down to 300 mK is depicted in Fig. 6. These results yield an upper critical field $\mu_0H_{c2}(0)$ of 7.5(5) T.

Resistivity measurements under hydrostatic pressure up to 12 kbar displayed in Fig. 7 reveal a linear decrease of the superconducting transition temperature T_c with $dT_c/dp=-130$ mK/kbar (see inset of Fig. 7) and significant pressure-induced changes of the normal state resistivity. As can be seen from Fig. 7, hydrostatic pressure of 12 kbar increases the residual resistivity ρ_0 by about 10%. The upper temperature range of the 12 kbar measurement (see the inset in Fig. 5) further reveals a significant reduction of the resistivity $\rho(T>100\ \mathrm{K})$ with respect to the results at ambient pressure. The analysis of these results in terms of the Bloch-Grüneisen law [see Eq. (1)] yields a pressure-induced increase of the Debye temperature Θ_D^ρ by about 5% (at 12 kbar). We note that these pressure-induced changes of $\rho(T)$ are strictly reversible within the accuracy of the experiment.

C. Specific heat measurements

The low-temperature specific heat of $\mathrm{La}_3\mathrm{Ni}_2\mathrm{B}_2\mathrm{N}_{3-\delta}$ determined for various external magnetic fields is shown in a C_p/T versus T^2 representation in Fig. 8. As demonstrated by the resistivity measurements (see Fig. 5) a magnetic field of 9 T is sufficient to suppress superconductivity to below 2 K. Thus, the 9 T measurement represents the normal state heat capacity $C_p=C_e+C_\mathrm{ph}\simeq\gamma T+\beta T^3$, where γ is the Sommerfeld parameter and β is related to the low-temperature value of the Debye temperature by $\Theta_D^\mathrm{LT}=(1944\times N/\beta)^{1/3}$ (N is the number of atoms per formula unit). From the low-temperature linear fit of the 9 T data ($10-30\ \mathrm{K}^2$) we obtain $\gamma=26(1)\ \mathrm{mJ/mol\ K}^2$ and $\Theta_D^\mathrm{LT}=303(3)$ K. The slope of the normal state specific heat, C_p/T versus T^2, changes significantly at about $40-50\ \mathrm{K}^2$, indicative of a low-temperature softening of acoustic phonon modes as also observed in $\mathrm{Nb}_3\mathrm{Sn}$.[16] The linear extrapolation of the normal state specific heat, C_p/T versus T^2, from above T_c yields an erroneously too high γ value of $37\ \mathrm{mJ/mol\ K}^2$; however, the interpretation of the corresponding slope in terms of an increased Debye temperature $\Theta_D=345$ K might reflect a temperature dependence of the low-energy phonon dispersion.

The idealization of the superconducting transition obeying the constraint of entropy conservation yields the height of the specific heat jump $(\Delta C)_{T_c}=(C_s-C_n)_{T_c}=0.43(2)\ \mathrm{J/mol\ K}$ and the thermodynamic mean value of the superconducting transition temperature $\overline{T_c}=11.7$ K. The normalized specific heat jump $(\Delta C)_{T_c}/\gamma T_c=1.4(1)$ coincides with the BCS value $(\Delta C)_{T_c}/\gamma T_c=1.43$.

In order to analyze the temperature dependence of the electronic specific heat in the superconducting state C_{eS}, we subtracted the phonon contributions C_ph (derived from the normal state heat capacity) from the zero-field measurement. The result is displayed in Fig. 9 in the usual semilogarithmic plot of the normalized electronic specific heat $C_{eS}/\gamma T_c$ ver-

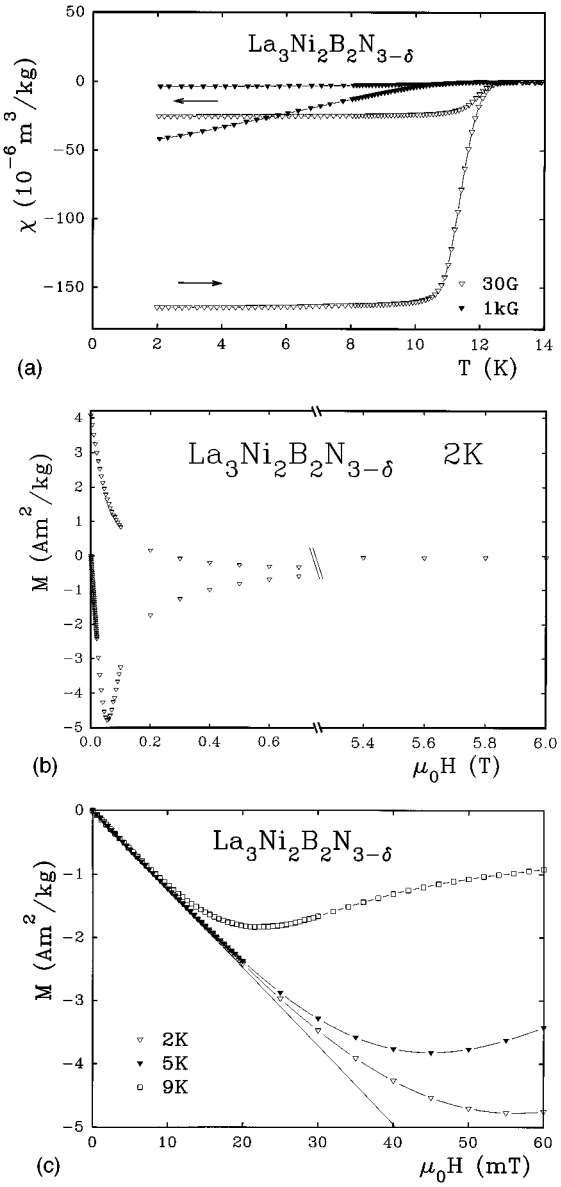

FIG. 4. (a)–(c) The temperature-dependent susceptibility of $La_3Ni_2B_2N_{3-\delta}$ subsequent to zero-field and field cooling as indicated by the arrows (a), the isothermal magnetization loop determined at 2 K (b), and the initial part of isothermal magnetization measurements (subsequent to zero-field cooling) taken at various temperatures as labeled (c).

sus T_c/T where we also include the data of $LuNi_2B_2C$ (taken from Ref. 17) for comparison and refer to a discussion of their different features in Sec. IV B.

The temperature dependence of C_{eS} in the BCS theory is given by the interpolation formula

$$C_{eS}(T)=8.5\gamma T_c\exp\left(-0.82\frac{\Delta_{\mathrm{BCS}}(0)}{k_BT}\right) \qquad (2)$$

for intermediate temperatures ($2.5<T_c/T<6$). Since C_{eS} of $La_3Ni_2B_2N_{3-\delta}$ exhibits an exponential temperature dependence rather than a power law as, e.g., for the borocarbides, Eq. 2 can be modified by replacing Δ_{BCS} by $\alpha\Delta_{\mathrm{BCS}}$ where $\alpha=\Delta(0)/\Delta_{\mathrm{BCS}}$ is a phenomenological parameter introduced to fit the experimental data. Thereby one obtains an experimental estimate for the gap to critical temperature ratio $\Delta(0)/k_BT_c$. As the accuracy of the experimental determination of C_{eS} is best for $2<T_c/T<3$ (i.e., $T=4$–6 K because $C_{eS}\sim C_{\mathrm{ph}}$), we use this temperature range to estimate $\Delta(0)/k_BT_c=1.85(5)$, yielding the dotted line in Fig. 9.

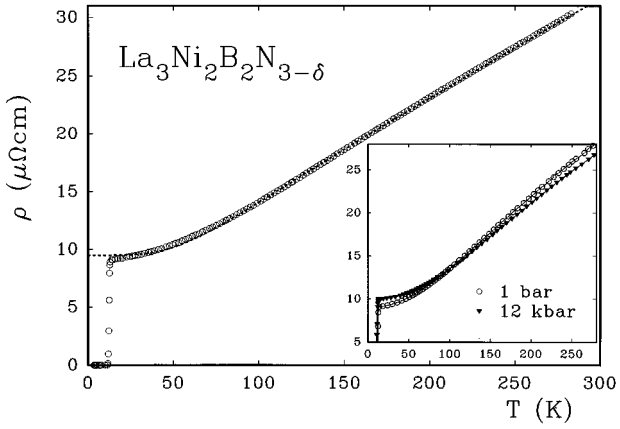

FIG. 5. The resistivity of $La_3Ni_2B_2N_{3-\delta}$ up to room temperature; the dotted line shows the Bloch-Grüneisen fit of the normal state resistivity. The results obtained with the liquid pressure cell are displayed in the inset.

For a more detailed investigation of the lattice properties of $La_3Ni_2B_2N_{3-\delta}$, we extended the heat capacity measurements up to room temperature (see Fig. 10) and analyzed the obtained specific heat contribution of the lattice vibrations by a similar procedure as described in Ref. 17 where a simple model phonon spectrum $F(\omega)$ was derived from the experimental specific heat of several borocarbide superconductors. As the lattice heat capacity of $La_3Ni_2B_2N_{3-\delta}$ provides no indication for low-energy Einstein modes, the number of free parameters could be reduced with respect to the analysis of RNi_2B_2C compounds. Thus, the model spectrum for $La_3Ni_2B_2N_3$ consists of a rather soft Debye spectrum and just two Gaussian contributions representing the 3 acoustic and 27 optical branches of the phonon spectrum, respectively. By analogy to the model spectrum used for the borocarbides (see Ref. 17), the high-energy Einstein contribution (Θ_{E_2}) is cut

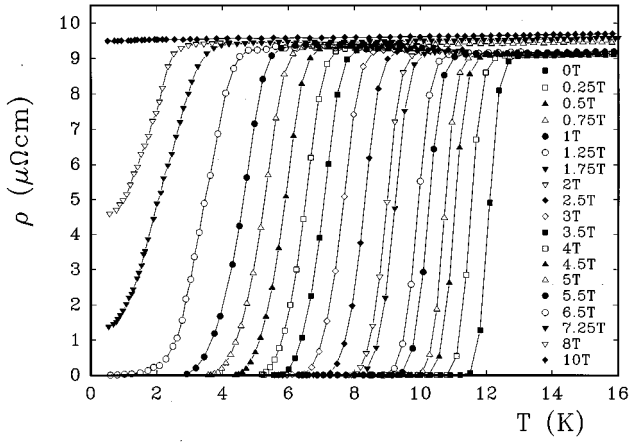

FIG. 6. The resistivity of $La_3Ni_2B_2N_{3-\delta}$ for various external magnetic fields as labeled.

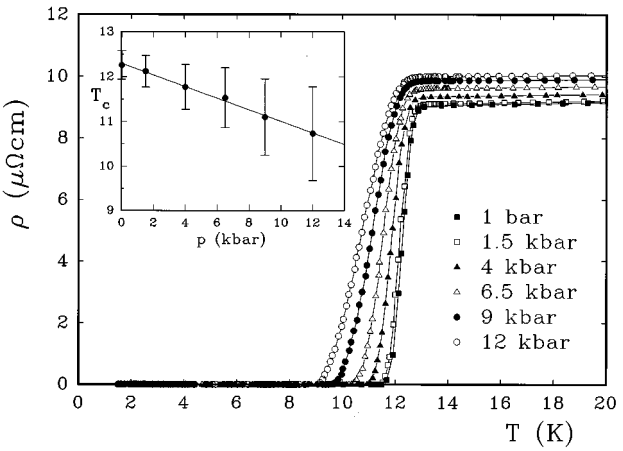

FIG. 7. Resistivity measurements under hydrostatic pressure as labeled; inset, the pressure dependence of the superconducting transition temperature T_c.

off at the peak position in order to obtain a high-energy limit. The ''hidden'' parameters of the model spectrum (adjusted by hand) are listed in Table II together with the ''characteristic frequencies'' obtained by a least squares fit. The overall features of the experimental 9 T data are reasonably well described by the heat capacity corresponding to the model spectra of $La_3Ni_2B_2N_{3-\delta}$ and $LuNi_2B_2C$ (Ref. 17) incorporating the normal state electronic contributions shown as solid lines in Fig. 10. However, the simple model spectrum of $La_3Ni_2B_2N_{3-\delta}$ does not provide such a satisfactory account for the low-temperature range as for $LuNi_2B_2C$ (see inset of Fig. 10). We emphasize that the model spectrum of $La_3Ni_2B_2N_{3-\delta}$ cannot be improved by including low-lying Einstein modes as is the case for the borocarbides. This might either arise from a temperature dependence of the low-energy phonon dispersion or from distinct detailed features of the low-energy phonon spectrum which are not properly described by the simple Debye spectrum.

The proposed model phonon density of states $F(\omega)$, however, yields sufficient information about the distribution of the spectral weight to evaluate the moments of the phonon spectrum. Spectral moments are suited to characterize $F(\omega)$ in a quite simple way (e.g., by the ratio $\omega_{\ln}/\overline{\omega_2}$; see

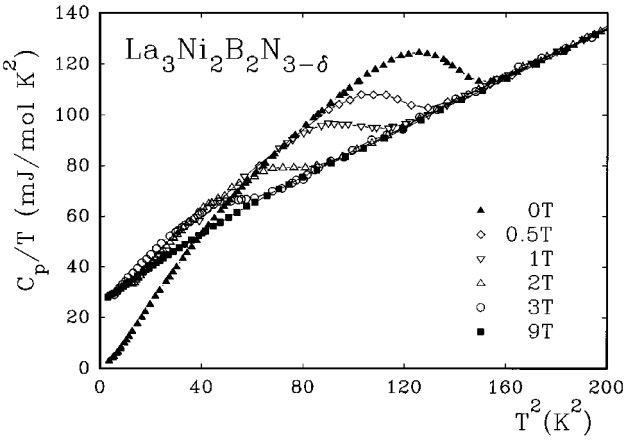

FIG. 8. The specific heat of $La_3Ni_2B_2N_{3-\delta}$ for various external magnetic fields as labeled.

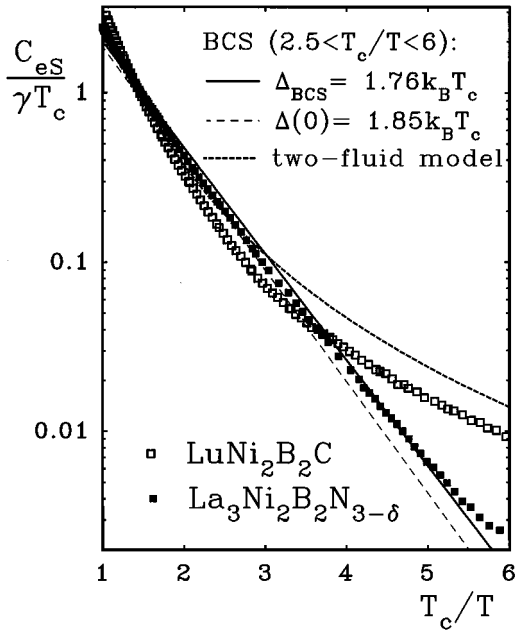

FIG. 9. The normalized electronic specific heat C_{eS} of $La_3Ni_2B_2N_{3-\delta}$ graphed as a function of the inverse reduced temperature T_c/T. The exponential temperature dependence according to BCS [with $\Delta(0)/k_BT_c=1.76$ and 1.85] and the result of the two-fluid model, $C_{eS}=3\gamma T_c(T/T_c)^3$, are shown by the solid and dashed lines, respectively. The normalized electronic specific heat of the borocarbide superconductor $LuNi_2B_2C$ is shown for comparison.

Ref. 18). As the shape of the electron-phonon spectral function $\alpha^2F(\omega)$ and that of the phonon spectrum, $F(\omega)$, is usually similar, we calculated the moments of the phonon spectrum, $\omega_{\ln}^p$, $\overline{\omega_1^p}$, and $\overline{\omega_2^p}$, according to the definition of the generalized moments $\omega_{\ln}$, $\overline{\omega_1}$, and $\overline{\omega_2}$ of the electron-phonon spectral function (see Ref. 18) taking $\alpha^2=1$. In the case of a frequency-independent electron-phonon matrix element $\alpha^2(\omega)$, the moments of $F(\omega)$ and $\alpha^2F(\omega)$ are identical. Hence, the superscript p refers to the special case of

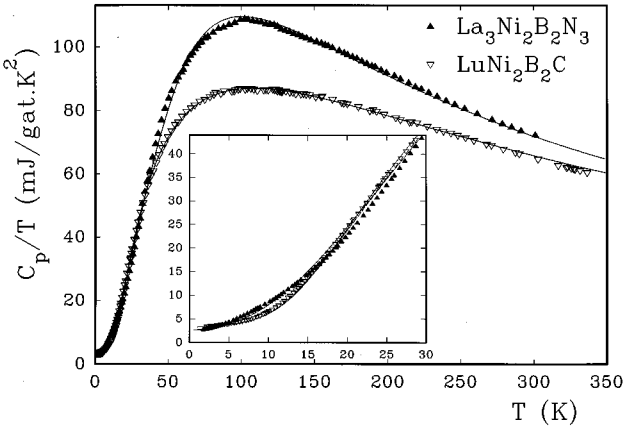

FIG. 10. The normal state specific heat of $La_3Ni_2B_2N_{3-\delta}$ and $LuNi_2B_2C$ (9 T data) up to room temperature. The solid lines show the heat capacities corresponding to the model phonon spectra (including the normal state electronic contributions).

TABLE II. The parameters of the model phonon spectrum $F(\omega)$.

Contribution	Θ_D	Θ_{E_1}	Θ_{E_2} (cutoff)
Width (K)		75	120
Weight	3	19	8
Position (K)	156	290	890

frequency-independent matrix elements $\alpha^2(\omega)$. The model phonon spectrum of $La_3Ni_2B_2N_{3-\delta}$ yields the average frequencies $\omega_{\ln}^p = 218$ K, $\overline{\omega_1^p} = 273$ K, and $\overline{\omega_2^p} = 333$ K which also enter the formula by Allen and Dynes[18] via the shape factor f_2 (see Sec. IV A).

D. Critical fields

1. Thermodynamic critical field

The temperature dependence of the thermodynamic critical field $H_c(T)$ shown in Fig. 11 is obtained by integrating the entropy difference between the normal and the superconducting states derived from the 0 T and 9 T data shown in the inset:

$$\frac{\mu_0 H_c^2(T)}{2} = \int_{T_c}^{T} \int_{T_c}^{T'} \frac{(C_s - C_n)}{T''} dT'' dT'. \tag{3}$$

The extrapolation of $\mu_0 H_c(T)$ to zero temperature gives the thermodynamic critical field $\mu_0 H_c(0) = 161(1)$ mT. Close to T_c we used the idealized data of the specific heat jump and obtained the slope of $\mu_0 H_c$ at T_c, $\mu_0 H_c'(T_c) = -24(1)$ mT/K, which satisfies the Rutgers formula[19] $(\Delta C)_{T_c} = \mu_0 (dH_c/dT)_{T_c}^2 T_c$ within the given error bars.

For a further analysis of the temperature dependence of $H_c(T)$ we graph in Fig. 12 the function $D(t) = h_c(t) - [1 - t^2]$ which describes the deviation of the normalized thermodynamic critical field $h_c(T) = H_c(T)/H_c(0)$ from a purely quadratic temperature dependence as a function of the reduced temperature $t = T/T_c$ squared. The maximal deviation of about -2% is of similar magnitude as predicted by the BCS weak-coupling theory (-3.8%). This indicates that the electron-phonon coupling strength of the boronitride superconductor $La_3Ni_2B_2N_{3-\delta}$ is close to the weak-coupling limit while the borocarbide superconductors are characterized as moderately strong-coupling superconductors due to their small positive or negative maximum values of the deviation function [YNi_2B_2C, -0.6% (Ref. 17) and -0.7% (Ref. 20), and $LuNi_2B_2C$ $+0.7\%$ (Ref. 17)].

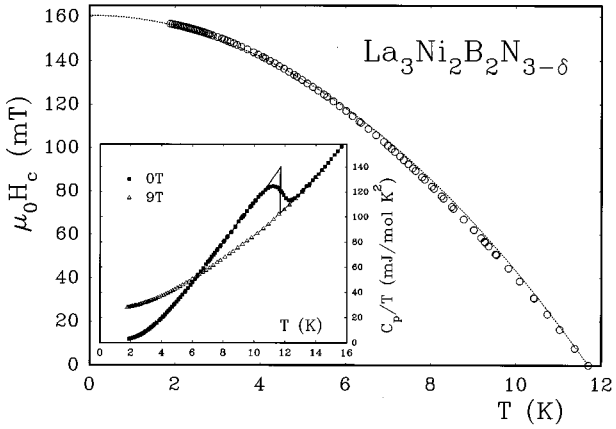

FIG. 11. The thermodynamic critical field $\mu_0 H_c(T)$ of $La_3Ni_2B_2N_{3-\delta}$. The dotted line shows the parabolic temperature dependence subtracted to obtain the deviation function; inset, the specific heat of $La_3Ni_2B_2N_{3-\delta}$ in the superconducting and normal state. The solid line accounts for an ideally sharp transition.

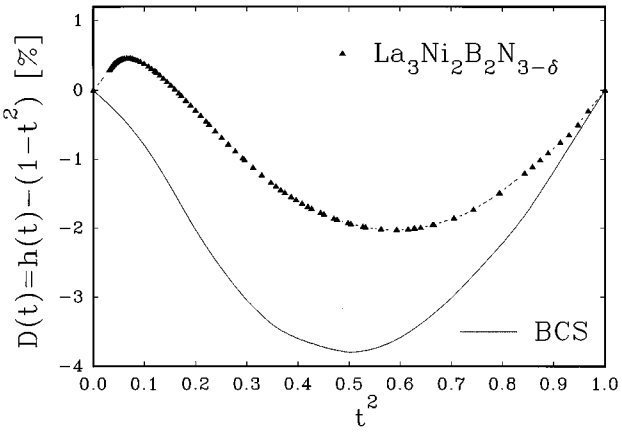

FIG. 12. The deviation function of the thermodynamic critical field $D(t) = H_c(t)/H_c(0)[1 - t^2]$ vs the reduced temperature $t = T/T_c$ squared.

2. Upper and lower critical field

The upper critical field $H_{c2}(T)$ was studied with resistivity and specific heat measurements. In the case of the resistivity measurements T_c is taken as the mean of the 10% and 90% resistive transition. Since the results of resistivity measurements might be influenced by surface effects, we performed a further evaluation of $H_{c2}(T)$ from the gradual shift of the specific heat anomaly with rising external magnetic fields displayed in Fig. 8 and additional measurements with fields ranging between 10 mT and 0.5 T. As mentioned above the transition temperature T_c was determined from an idealized sharp specific heat jump under the constraint of entropy conservation. As external magnetic fields up to 300 mT hardly alter the shape of the specific heat anomaly, these measurements yield a reliable value for the initial slope of H_{c2} at T_c, $\mu_0 H_{c2}'(T_c) = -0.37(6)$ T/K which is nearly independent from the particular way of evaluating T_c. An estimation of $\mu_0 H_{c2}(0)$ with the Werthamer formula yields $\mu_0 H_{c2}(0) = 0.7 \mu_0 H_{c2}'(T_c) T_c \sim 3$ T, a value significantly smaller than that obtained from the high-field resistivity measurements [$\mu_0 H_{c2}(0) = 7.5(5)$ T].

The temperature dependence of H_{c2} obtained from specific heat and resistivity measurements is shown in Fig. 13. The dashed line corresponds to the clean limit calculations of Helfand and Werthamer[21] rescaled to fit the experimental data. As can be seen from this comparison, $H_{c2}(T)$ exhibits a significant decrease of the slope below 2 T which is reminiscent of the borocarbide superconductors and remains to be resolved.

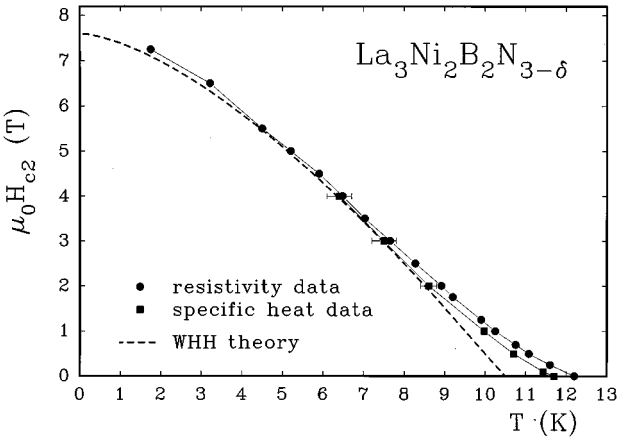

FIG. 13. The upper critical field of $La_3Ni_2B_2N_{3-\delta}$ obtained from specific heat and resistivity measurements; dashed line, (scaled) temperature dependence of H_{c2} according to Helfand and Werthamer (Ref. 21) (labeled as WHH theory).

The temperature dependence of the lower critical field H_{c1} obtained from isothermal magnetization measurements (see Sec. III B) is shown in Fig. 14. A BCS fit which can simply be approximated by a $[1-(T/T_c)^{3/2}]$ dependence yields a low-temperature extrapolation of the lower critical field $\mu_0 H_{c1}(0)=13(2)$ mT.

E. Ginzburg-Landau parameter κ and the characteristic lengths ξ and λ

The above-described extrapolations of the thermodynamic and the upper critical fields $H_c(0)$ and $H_{c2}(0)$ are used to determine the ratio of the spatial variation length of the local magnetic field $\lambda_{GL}(0)$ to the coherence length $\xi_{GL}(0)$ via Abrikosov's relation $\lambda_{GL}(0)/\xi_{GL}(0)\equiv\kappa_{GL}(0)=H_{c2}/[\sqrt{2}H_c(0)]$ from which we obtain the Ginzburg-Landau parameter $\kappa_{GL}=33(2)$ for $La_3Ni_2B_2N_{3-\delta}$.

The absolute values of the coherence length ξ_0 and the penetration depth $\lambda(0)$ can be evaluated with the basic equations of the isotropic Ginzburg-Landau-Abrikosov-Gor'kov (GLAG) theory:

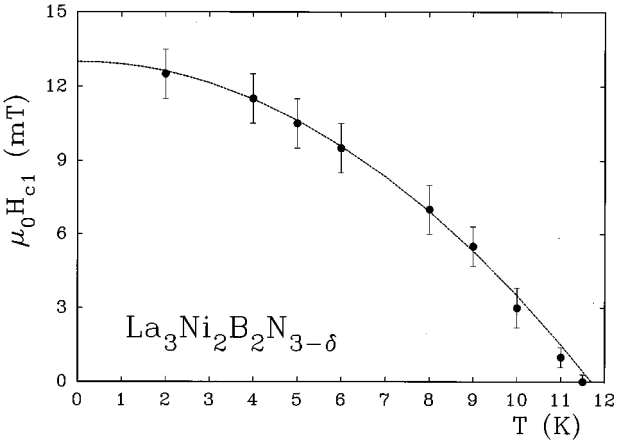

FIG. 14. The lower critical field of $La_3Ni_2B_2N_{3-\delta}$ determined with isothermal magnetization measurements. The extrapolation of H_{c1} to zero temperature by a $[1-(T/T_c)^{3/2}]$ dependence is indicated by the dotted line.

TABLE III. The basic quantities describing the thermodynamic properties of the superconducting state of $La_3Ni_2B_2N_{3-\delta}$.

$\overline{T_c}$	11.7 K
γ	26(1) mJ/mol K^2
Θ_D^{LT}	303(3) K
$(\Delta C)_{T_c}$	0.43(2) J/mol K
$\mu_0 H_c(0)$	161(1) mT
$\Delta C/\gamma T_c$	1.4(1) (BCS: 1.43)
$\gamma T_c^2/H_c^2(0)$	0.159(6) (BCS: 0.168)
$H_c(0)/H_c'(T_c)T_c$	0.573(10) (BCS: 0.576)
$\Delta(0)/k_B T_c$	1.85(5) (BCS: 1.76)
$\mu_0 H_{c1}(0)$	13 (2) mT
$\mu_0 H_{c2}(0)$	7.5 (5) T
$\kappa_{GL}(0)$	33 (2)
$\xi_{GL}(0)$	7.0 (5) nm
$\lambda_{GL}(0)$	213 (10) nm

$$\kappa(T)=\frac{2\pi\sqrt{2}\mu_0 H_c(T)\lambda_{GL}^2(T)}{\Phi_0}, \tag{4}$$

$$H_{c2}(T)=\frac{\Phi_0}{2\pi\mu_0\xi_{GL}^2(T)}, \tag{5}$$

$$H_{c1}(T)=\frac{\Phi_0}{4\pi\mu_0\lambda_{GL}^2(T)}\ln\kappa, \tag{6}$$

with $\Phi_0=h/2e$ the fluxoid quantum.

The first two relations are used to determine the characteristic lengths $\xi_{GL}(0)$ and $\lambda_{GL}(0)$ from the experimental results of $H_c(0)$ and $H_{c2}(0)$ and the third one yields a proof for the consistency of the data set obtained. It has to be noted that although the GLAG theory is valid in the vicinity of T_c, the basic conclusions are valid at any temperatures.[22] The use of the isotropic formulas is justified by the band structure results by Singh and Pickett[9] and Mattheiss,[10] which indicate that the electronic properties of $La_3Ni_2B_2N_{3-\delta}$ are rather isotropic.

The values for $\xi_{GL}(0)$ and $\lambda_{GL}(0)$ are collected in Table III together with the experimental results characterizing the thermodynamics of the superconducting state in $La_3Ni_2B_2N_{3-\delta}$. Good agreement is obtained between $H_{c1}=12.7$ mT calculated from Eq. (6) and the experimental value 13(2) mT derived from magnetization measurements.

IV. DISCUSSION

A. Electron-phonon coupling strength

A comparison of the thermodynamic ratios $\Delta C/\gamma T_c$ and $H_c(0)/H_c'(T_c)T_c$ with the values predicted by the weak-coupling (BSC) theory (see Table III) shows rather good agreement within the given error. Moderate deviations from the universal BCS values are obtained for the ratios $\gamma T_c^2/H_c^2(0)$ and $\Delta(0)/k_B T_c$. As already discussed above, a small deviation from the weak-coupling predictions is also evident from the shape of the function $D(t)$. Within the phenomenological α model by Padamsee *et al.*[23] the shape of

the deviation function $D(t)$ of $La_3Ni_2B_2N_{3-\delta}$ is correlated to a gap to critical temperature ratio $\Delta(0)/k_BT_c=1.9$ which is slightly larger than the value estimated from an exponential fit to the electronic specific heat $C_{eS}(T)$.

The discussion of the electron-phonon coupling strength in terms of the strong-coupling parameter $T_c/\omega_{\ln}$ requires a reliable determination of the logarithmic moment of the electron-phonon spectral function $\alpha^2F(\omega)$. For the borocarbide superconductors[17] $\omega_{\ln}$ could be estimated via the approximate relations by Carbotte.[24] For $La_3Ni_2B_2N_{3-\delta}$ the strong-coupling corrections to the thermodynamic ratios are rather small; nevertheless, the moderate deviation of the ratios $\gamma T_c^2/H_c^2(0)$ and $\Delta(0)/k_BT_c$ from their BCS values yields an upper limit for the ratio $T_c/\omega_{\ln}\leqslant 0.05$ and accordingly a lower limit for the moment $\omega_{\ln}\geqslant 235$ K, being slightly higher but of same magnitude as the pure phonon moment $\omega_{\ln}^p=218$ K derived from the model spectrum. The estimate of the lower limit $\omega_{\ln}\geqslant 235$ K is in agreement with the empirical relation $\omega_{\ln}\approx 0.83\Theta_D$ proposed by Dynes[25] which yields $\omega_{\ln}\approx 251$ K for $La_3Ni_2B_2N_{3-\delta}$. In this context it is important to note that for the borocarbide superconductors a similar estimation of $\omega_{\ln}$ using the Debye temperature Θ_D^{LT} yields significantly too large values $\omega_{\ln}$ and thus too small ratios $T_c/\omega_{\ln}$ which are not sufficient to account for the strong-coupling corrections to the thermodynamic ratios.

The thermodynamic properties of the superconducting state characterize $La_3Ni_2B_2N_{3-\delta}$ as a typical weak-coupling BCS superconductor. However, the transition temperature $T_c=11.7$ K is rather large among intermetallic superconductors. Thus, it is worth evaluating the electron-phonon mass enhancement λ with the McMillan formula[26]

$$T_c=\frac{\Theta_D}{1.45}\exp\left(-\frac{1.04(1+\lambda)}{\lambda-\mu^\star(1+0.62\lambda)}\right). \tag{7}$$

Taking $\mu^\star=0.1$–0.13 we obtain $\lambda=0.8$–0.9, which is in good agreement with an estimation of the mass enhancement $\lambda\equiv\gamma/\gamma_{bs}-1=0.85$ resulting from a comparison of the experimental γ value with the γ value corresponding to the bare density of states calculated by Mattheiss,[10] who obtained $\gamma_{bs}=14$ mJ/mol K^2 for $La_3Ni_2B_2N_3$. Note that $\lambda\approx 0.85$ can also be obtained via the formula by Allen and Dynes[18] (using $\omega_{\ln}=251$ K) because for $La_3Ni_2B_2N_3$ ($\overline{\omega_2^p}/\omega_{\ln}^p\sim 1.5$) the corrective factors to the McMillan formula are close to 1, while these are significantly larger for the borocarbides.[17] Hence, we emphasize that both the McMillan and the Allen-Dynes formulas are appropriate for $La_3Ni_2B_2N_{3-\delta}$ while for the borocarbides only the Allen-Dynes formula provides satisfactory description.

B. Comparison of $La_3Ni_2B_2N_{3-\delta}$ with the borocarbide superconductors

The compounds $(LaN)_nNi_2B_2$ ($n=2$, 3) were found to be isostructural with the homologous series $(RC)_mNi_2B_2$ ($R=$Y, Lu and $m=1,\ \ldots\ ,4$);[5] thus it is illuminating to discuss the physical properties of the boronitride with respect to the borocarbide superconductors.

The analysis of the thermodynamic properties of the superconducting state of $La_3Ni_2B_2N_3$ and, e.g., $LuNi_2B_2C$ (Ref. 17), in terms of the dimensionless BCS ratios $\Delta C/\gamma T_c$, $\gamma T_c^2/H_c^2(0)$, $H_c(0)/H_c'(T_c)T_c$, and $\Delta(0)/k_BT_c$ shows that $La_3Ni_2B_2N_{3-\delta}$ fits well to the BSC weak-coupling predictions (see Table III) whereas the borocarbides are moderately strong-coupling superconductors and the deviation of their thermodynamic ratios from the BCS values due to strong-coupling effects is described satisfactorily in terms of the strong-coupling parameter $T_c/\omega_{\ln}$ ranging between 0.06 and 0.1.[17] For $La_3Ni_2B_2N_3$ we estimate $T_c/\omega_{\ln}$ to be below 0.05 which is close to the weak-coupling limit. A further significant difference emerges from a comparison of the electronic specific heat C_{eS} displayed in Fig. 9 (see Sec. III C). The electronic heat capacity of $La_3Ni_2B_2N_{3-\delta}$ exhibits an exponential temperature dependence as predicted by the BCS theory while that of $LuNi_2B_2C$ and related borocarbide superconductors (see, e.g., Refs. 27 and 28) follows a power law with an exponent close to 3. The latter may be attributed to strong-coupling effects and/or to gapless regions at the Fermi surface.

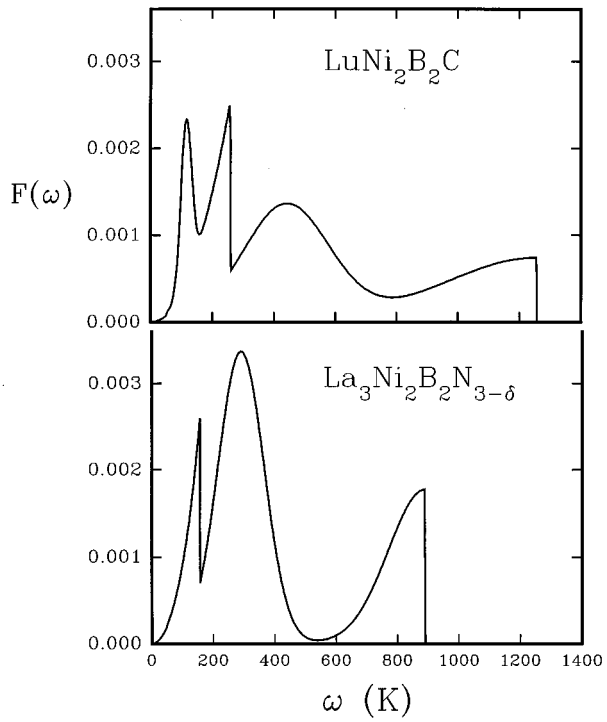

FIG. 15. Comparison of the model phonon spectrum of $La_3Ni_2B_2N_{3-\delta}$ with that of the borocarbide superconductor $LuNi_2B_2C$. Both spectra are normalized to 1.

According to the above-mentioned results it is obvious that $La_3Ni_2B_2N_3$ should be classified as a typical weak-coupling superconductor; however, an estimation of the electron-phonon coupling strength (see Sec. IV A) shows that the electron-phonon mass enhancement $\lambda\sim 0.85$ is only slightly smaller than that of YNi_2B_2C ($\lambda\sim 0.95$).[17] Since the thermodynamic properties of the superconducting state are related to particular features of the Eliashberg function $\alpha^2F(\omega)$, it is instructive to compare the model phonon spectra of $La_3Ni_2B_2N_{3-\delta}$ and $LuNi_2B_2C$ (Ref. 17) displayed in Fig. 15.

The significant difference between the two model spectra is twofold: A remarkable reduction of the high-energy opti-

cal modes of $La_3Ni_2B_2N_{3-\delta}$ with respect to those of the single-layer borocarbides which can be attributed to the absence of the rigid B-C-B chains in the former. Second, the pronounced low-energy Einstein contribution ($\Theta_{E1} < \Theta_D$) situated within the Debye spectrum, which appears to be typical for the borocarbides RNi_2B_2C (R=Y, La, Lu) and $LaPt_{1.5}Au_{0.5}B_2C$,[17] could not be resolved in our analysis of $La_3Ni_2B_2N_{3-\delta}$. In particular, with respect to the low-lying Einstein modes inelastic neutron scattering (INS) measurements by Dervenagas *et al.*[29] support our model phonon spectra of the borocarbides: The low-lying phonon dispersion curves of $LuNi_2B_2C$ along the $[\xi 00]$ and $[00\xi]$ high-symmetry directions provide evidence that the low-energy maximum of $F(\omega)$ of $LuNi_2B_2C$ at $\omega \sim 120$ K correlates to a transverse optical phonon branch (Δ_4) and to a flat part of the transverse acoustic branches. Dervenagas *et al.*[29] further reported a significant low-temperature softening of these two phonon branches in the vicinity of the zone-boundary point G_1, indicative of a pronounced interaction between these particular phonons and conduction electrons. We note that the lattice heat capacity of $LuNi_2B_2C$ and related borocarbides does not give any hint of phonon softening below T_c while such a feature may be anticipated from the low-temperature heat capacity of $La_3Ni_2B_2N_{3-\delta}$ (see below). This apparent discrepancy between specific heat and INS results for the borocarbide superconductor $LuNi_2B_2C$ is probably caused by the rather small Brillouin zone areas where phonon softening is closely related to a nesting feature at the Fermi surface.[30]

For $La_3Ni_2B_2N_{3-\delta}$, however, the downward bending of the normal state specific heat in the C_p/T versus T^2 plot below $T \sim T_c/2$ indicates a reduction of Θ_D^{LT} by more than 10% (see Sec. III C), implying a low-temperature softening of the acoustic phonon modes. As this heat capacity feature is just opposite to that observed for the borocarbides[17] we suggest that either the low-energy Einstein modes present in the borocarbides mask the phonon softening in the heat capacity data and/or that the softening of acoustic phonon modes in $La_3Ni_2B_2N_{3-\delta}$ involves not only modes at the Brillouin zone boundary but also those with smaller wave vectors which primarily determine the low-temperature heat capacity. The latter implies that the phonon softening should be more isotropic in k space for $La_3Ni_2B_2N_{3-\delta}$ than in the case of $LuNi_2B_2C$ and the related borocarbides. On the other hand the downward bending of the heat capacity in the C_p/T versus T^2 plot might also be caused by distinct details of the low-energy phonon spectrum of $La_3Ni_2B_2N_{3-\delta}$.[31]

The effect of hydrostatic pressure upon T_c of $La_3Ni_2B_2N_{3-\delta}$ and the borocarbides provides further information about the phononic and electronic properties of these compounds. In general, pressure dependences of T_c are mainly caused by two effects: First, the volume compression generally gives rise to a lattice stiffening, yielding an increase of the mean phonon frequency and, second, causes a broadening of the bandwidth concomitant with a change of $N(E_f)$ either in the positive or negative direction. Both quantities, the mean phonon frequency $\overline{\omega_2}$ and $N(E_f)$, enter the McMillan formula for T_c [Eq. (7)] via the electron-phonon coupling strength parameter $\lambda = N(E_f)\langle I^2\rangle/(M\overline{\omega_2^2})$ with $\langle I^2\rangle$ the average of the electron-phonon matrix elements and M the mean atomic mass. Thus, in a first approach ignoring the pressure dependence of $\langle I^2\rangle$ and μ^*, the effect of pressure-induced lattice stiffening leads usually to a decrease of T_c, whereas electronic changes may either give rise to an increase or to a decrease of T_c depending on whether $N(E_f)$ is enhanced or reduced.

Resistivity measurements under hydrostatic pressure up to 12 kbar (see Sec. III B) reveal a significant reduction of T_c for $La_3Ni_2B_2N_{3-\delta}$ with an initial slope $dT_c/dp = -130$ mK/kbar that is about one order of magnitude larger than the corresponding dT_c/dp values of the borocarbide superconductors as, e.g., $LuNi_2B_2C$ [+18 mK/kbar (Ref. 32)] and YNi_2B_2C [+3 mK/kbar (Ref. 33), −6 mK/kbar (Ref. 33), and −9 mK/kbar (Ref. 34)]. From the analysis the normal state resistivity in terms of a simple Bloch-Grüneisen law we obtained an increase of $\Theta_D^p(p)$ by about 5% at 12 kbar for $La_3Ni_2B_2N_{3-\delta}$ (see Sec. III B) which we use as a first estimate for the stiffening of the mean phonon frequency $\overline{\omega_2}$ and Θ_D under hydrostatic pressure. In terms of the McMillan formula these purely phononic changes yield $dT_c/dp \sim -150$ mK/kbar, being of the same magnitude as the experimentally determined value $dT_c/dp = -130$ mK/kbar. This agreement indicates that electronic effects play a minor role; i.e., pressure-induced changes of $N(E_f)$ are rather small for $La_3Ni_2B_2N_{3-\delta}$. Hence, under the assumption of similar compressibilities for both the borocarbides and $La_3Ni_2B_2N_{3-\delta}$ phononic changes alone cannot account for the small positive or negative pressure dependence of T_c observed for the borocarbides. In this context it is worth noting that not only the compressibility of YNi_2B_2C $d\ln V/dp = -0.82(8)\times 10^{-3}$ kbar^{-1} but also its anisotropy with respect to the a and c axes ($d\ln a/dp = -0.22\times 10^{-3}$ kbar^{-1}, $d\ln c/dp = -0.4\times 10^{-3}$ kbar^{-1}) (Ref. 35) is practically the same for $CeCu_2Si_2$ (Ref. 36) and $CeRu_2Si_2$ (Ref. 37), with the unfilled $ThCr_2Si_2$ structure where the rigid B-C-B chains are missing. This is unexpected since the chemical pressure due to the lanthanide contraction causes an anomalous counteracting variation of the a and c axes across the RNi_2B_2C series while in the RCo_2B_2 series with the unfilled $ThCr_2Si_2$ structure both the a and c parameters show the usual lanthanide contraction.[38] The intriguing anomaly of the c and a axis variation was successfully explained in terms of a structural model where the B-Ni-B bond angle accommodates the strain produced by a growing size of the rare-earth ions in the RC layer. This causes a reduction of the c axis while the a axis expands if one proceeds from Lu to La in this series.[38]

As superconductivity is proposed to be associated with the optimal B-Ni-B tetrahedral angle of about 109° which moves sp levels down to the Fermi level giving rise to high $N(E_f)$,[40] hydrostatic pressure may affect this angle in a different way in the borocarbides and $La_3Ni_2B_2N_{3-\delta}$. Thus, an interpretation of the distinct pressure effects upon T_c differing by one order of magnitude between $La_3Ni_2B_2N_{3-\delta}$ and the borocarbides remains speculative due to the lack of elastic constants of the former. However, under the assumption of similar compressibilities for both systems, the small positive or negative dT_c/dp values of the borocarbides indicate that electronic changes compensate the effect of lattice stiff-

ening under external pressure which seems to be the dominant effect in $La_3Ni_2B_2N_{3-\delta}$.

V. CONCLUSION

Magnetization, resistivity, and specific heat measurements were carried out on thoroughly prepared $La_3Ni_2B_2N_{3-\delta}$ characterized by x-ray diffraction, electron microprobe analysis, and high-resolution electron microscopy. The results obtained for the three critical fields allow the classification of $La_3Ni_2B_2N_{3-\delta}$ as a typical hard type-II superconductor with a Ginzburg-Landau parameter $\kappa_{GL}=33(2)$, a coherence length $\xi_{GL}(0)=7.0(5)$ nm, and a penetration depth $\lambda_{GL}(0)=210(10)$ nm. According to the small deviation of the four thermodynamic ratios $\Delta C/\gamma T_c$, $\gamma T_c^2/H_c^2(0)$, $H_c(0)/H_c'(T_c)T_c$, and $\Delta(0)/k_BT_c$ from their universal BCS values $La_3Ni_2B_2N_{3-\delta}$ can be regarded as a weak-coupling BCS superconductor although the estimate of the electron-phonon mass enhancement $\lambda\sim0.85$ is of comparable magnitude as that of the moderately strong coupling, YNi_2B_2C ($\lambda\sim0.95$), which, however, shows together with the other superconducting borocarbides significantly different thermodynamic characteristics. This is also manifested by the electronic specific heat of $La_3Ni_2B_2N_{3-\delta}$ following the usual BCS exponential behavior while that of the borocarbides can be described by a power law with an exponent close to 3 which may be attributed to strong-coupling effects and/or to gapless regions at the Fermi surface.

A comparison between the lattice heat capacities of $La_3Ni_2B_2N_{3-\delta}$ and the borocarbide superconductors reveals distinctly different features of the model phonon density of states $F(\omega)$. In particular with respect to the low-energy part of the phonon spectra we suggest for $La_3Ni_2B_2N_{3-\delta}$ that the Debye spectrum is dominating while for the borocarbides additional low-lying Einstein modes are present. The latter is in agreement with a phonon softening of low-lying acoustic and optical branches observed by inelastic neutron scattering on $LuNi_2B_2C$.[29]

The pressure dependence of T_c ($dT_c/dp=-130$ mK/kbar) in $La_3Ni_2B_2N_{3-\delta}$ is found to be one order of magnitude larger than that of the borocarbides and in a first attempt can be explained in terms of the McMillan formula by a lattice stiffening derived from the pressure dependence of the normal state resistivity while under the assumption of similar compressibilities of the borocarbides electronic changes seem to compensate the effect of the pressure-induced lattice stiffening upon T_c in the latter.

Finally, the significantly different thermodynamic properties of the borocarbide and boronitride superconductors show that despite the layered crystal structure (triple LaN layers separating the Ni_2B_2 layers) $La_3Ni_2B_2N_{3-\delta}$ is a rather isotropic superconductor and its electron-phonon interactions are more BCS-like than in the borocarbides.

ACKNOWLEDGMENTS

Thanks are due to Dr. M. Bohn for the wavelength dispersive spectrography at the Centre de la Microsonde Electronique de l'anest, IFREMER, Plonzan, Brest. P.R. wants to express his gratitude to the Austrian Academy of Sciences for some support under Grant No. PICS-134. This work was supported by the Austrian Science Foundation under Grant Nos. P11090 and P10269 and by the Kärntner Elektrizitätsgesellschaft (KELAG).

[1] R. J. Cava, H. Takagi, H. W. Zandbergen, J. J. Krajewski, W. F. Peck, Jr., T. Sigrist, B. Batlogg, R. B. van Dover, R. J. Felder, K. Mizuhashi, J. O. Lee, H. Eisaki, and S. Uchida, Nature (London) **367**, 254 (1994).

[2] R. J. Cava, H. Takagi, B. Batlogg, H. W. Zandbergen, J. J. Krajewski, W. F. Peck, Jr., R. B. van Dover, R. J. Felder, T. Siegrist, K. Mizuhashi, J. O. Lee, H. Eisaki, S. A. Carter, and S. Uchida, Nature (London) **367**, 146 (1994).

[3] R. Nagarajan, C. Mazumdar, Z. Hossain, S. K. Dhar, K. V. Gopalakrishnan, L. C. Gupta, C. Godart, B. D. Padalia, and R. Vijayaraghavan, Phys. Rev. Lett. **72**, 274 (1994).

[4] R. J. Cava, H. W. Zandbergen, B. Batlogg, H. Eisaki, H. Takagi, J. J. Krajewski, W. F. Peck, Jr., E. M. Gyorgy, and S. Uchida, Nature (London) **372**, 245 (1994).

[5] H. W. Zandbergen, J. Jansen, R. J. Cava, J. J. Krajewski, and W. F. Peck, Jr., Nature (London) **372**, 759 (1994).

[6] T. Siegrist, H. W. Zandbergen, R. J. Cava, J. J. Krajewski, and W. F. Peck, Jr., Nature (London) **367**, 146 (1994).

[7] Li Rukang, X. Chaoshui, Z. Hong, Lu Bin, and Yang Li, J. Alloys Compounds **223**, 53 (1995).

[8] A. K. Gangopadhyay and J. S. Schilling, Phys. Rev. B (to be published).

[9] D. J. Singh and W. E. Pickett, Phys. Rev. B **51**, 8668 (1995).

[10] L. F. Mattheiss, Solid State Commun. **94**, 741 (1995).

[11] J. L. Pouchon and F. Pichoir, J. Microscop. Spectrosc. Electron. **10**, 279 (1985).

[12] Q. Huang, B. C. Chakoumakos, A. Santoro, R. J. Cava, J. J. Krajewski, and W. F. Peck, Jr., Physica C **244**, 101 (1995).

[13] P. Rogl, in *Inorganic Reactions and Methods*, edited by J. J. Zuckerman (VCH Publications, Weinheim, 1991), Vol. 13, Chap. 6, pp. 85–161.

[14] P. Rogl, in *The Physics and Chemistry of Carbides, Nitrides and Borides*, edited by R. Freer (Kluwer Academic, Dordrecht, The Netherlands, 1990), pp. 269–277.

[15] E. Parthé and L.M. Gelato, Acta Crystallogr. A **41**, 142 (1985).

[16] G. R. Steward, B. Cort, and G. W. Webb, Phys. Rev. B **24**, 3841 (1981).

[17] H. Michor, T. Holubar, C. Dusek, and G. Hilscher, Phys. Rev. B **52**, 16 165 (1995).

[18] P. B. Allen and R. C. Dynes, Phys. Rev. B **12**, 905 (1975).

[19] A. J. Rutgers, Physica **3**, 999 (1936).

[20] R. Movshovich, M. F. Hundley, J. D. Thompson, P. C. Canfield, B. K. Cho, and A. V. Chubukov, Physica C **227**, 381 (1994).

[21] E. Helfand and N. R. Werthamer, Phys. Rev. **147**, 288 (1966); N. R. Werthamer, E. Helfand, and P. C. Hohenberg, *ibid.* **147**, 295 (1966).

[22] A. A. Abrikosov, *Fundamentals of the Theory of Metals* (North-Holland, Amsterdam, 1988).

[23] H. Padamsee, J. E. Neighbor, and C. A. Shiffman, J. Low Temp. Phys. **12**, 387 (1973).

[24] J. P. Carbotte, Rev. Mod. Phys. **62**, 1027 (1990).

[25] R. C. Dynes, Solid State Commun. **10**, 615 (1972).
[26] W. L. McMillan, Phys. Rev. **167**, 331 (1968).
[27] N. M. Hong, H. Michor, M. Vybornov, T. Holubar, P. Hundegger, W. Perthold, G. Hilscher, and P. Rogl, Physica C **227**, 85 (1994).
[28] S. A. Carter, B. Batlogg, R. J. Cava, J. J. Krajewski, and W. F. Peck, Jr., Phys. Rev. B **50**, 4216 (1994).
[29] P. Dervenagas, M. Bullock, J. Zarestky, P. Canfield, B. K. Cho, B. Harmon, A. I. Goldman, and C. Stassis, Phys. Rev. B **52**, 9839 (1995).
[30] W. Weber (unpublished).
[31] W. Reichardt (private communication).
[32] H. Schmidt and H. F. Braun, Physica C **229**, 315 (1994).
[33] E. Alleno, J. J. Neumeier, J. D. Thompson, P. C. Canfield, and B. K. Cho, Physica C **242**, 169 (1995).
[34] C. Looney, A. K. Gangopadhyay, A. K. Klehe, and J. S. Schilling, Physica C **252**, 199 (1995).
[35] S. L. Bud'ko, G. B. Demishev, M. B. Fontes, and E. Baggio-Saitovitch, J. Phys. Condens. Matter **8**, L159 (1996).
[36] F. Steglich, J. Magn. Magn. Mater. **100**, 186 (1991).
[37] P. Haen, J.-M. Laurent, K. Payer, and J.-M. Mignot, in *Transport and Thermal Properties of f-Electron Systems*, edited by G. Oomi *et al.* (Plenum, New York, 1993), p. 145.
[38] P. Villars and L. D. Calvert, *Pearson's Handbook of Crystallographic Data for Intermetallic Phases* (AMS Int., Materials Park, OH, 1991), Vols. 1–4.
[39] T. Siegrist, R. J. Cava, J. J. Krajewski, and W. F. Peck, Jr., J. Alloys Compounds **216**, 135 (1994).
[40] L. F. Mattheiss, Solid State Comm. **91**, 587 (1994).